Fission fragment angular distribution in alpha-particle-induced fission of actinide elements

R K JAIN, S K BOSE and J RAMA RAO
Department of Physics, Banaras Hindu University, Varanasi 221 005, India

Abstract. Using Lexan polycarbonate plastic as the fission fragment track detectors, the fragment angular distributions have been measured in the cases of fission of ^{232}Th and ^{238}U induced by alpha particles of various energies ranging from 40 to 70 MeV obtained from the 88″ variable energy cyclotron at Calcutta. The center-of-mass angular distributions have been calculated and fitted by a series of Legendre polynomials. The $W(10°)/W(90°)$ ratios (defined as anisotropy) were measured at several energies for both the targets. These data are utilized in calculation of the energy dependence of K_0^2, the standard deviation of the distribution in the angular momentum projection on the nuclear symmetry axis at the saddle point. Values of Γ_f/Γ_n, i.e. the ratio of the fission width to neutron emission width have been determined for ^{232}Th and ^{238}U nuclei. The integral cross-section for alpha induced fission in each target was determined by numerical integration of the respective center-of-mass angular differential cross-sections. The results were compared with similar data available in the literature which served to resolve some of the discrepancies observed in earlier measurements. The results were also compared with theoretical cross-sections.

1. Introduction

The present investigations on fission fragment angular distributions are undertaken to study the saddle point configuration and the competition between fission and neutron evaporation. Several measurements on the fission cross-section and fragment angular distribution in the fission of a number of nuclei induced by a variety of projectiles have been reported, a few of them using SSNTDs (Solid State Nuclear Track Detectors) [1–7]. The interpretation of the observed angular distributions and the important inferences drawn from them, are all primarily based on the model proposed by Bohr [8]. The underlying idea of the model is that the stretched fission nucleus, in passing over the saddle point, exhibits quantum states similar to those observed in the permanently deformed nuclei, except that the states of the saddle point nucleus are expected to be quasi-stationary since the nucleus only stays a while at the saddle point. Then the angular distribution of the fragments depends on the available quantum states characterized by I, M and K, where I is the total angular momentum of the nucleus, M is the projection of I on a space fixed axis (taken as the incident beam direction) and K is the projection of I on the symmetry axis of

519

the fissioning nucleus. By assuming that K is conserved from saddle point to scission point, the expected angular distribution of the fission fragments can be calculated by averaging over the distribution of the I, M and K states available at the saddle point. M is usually zero for particle induced fission [9].

Another interesting information, the angular distribution study can yield, is about the dissipation of the large angular momentum brought in by the incident particle into the fissioning system. The simple classical model of Coffin and Halpern [3], is useful for letting one see qualitatively what sort of insight can be obtained. In three dimensions one would observe the number of fragments per unit solid angle to be $dN/\sin\theta\, d\theta$, which would consequently be proportional to $(\sin\theta)^{-1}$. The angular distribution peaks very sharply in the forward and backward directions (figure 3). Thus if a major fraction of the 'input' angular momentum were to feed into the orbital momentum between the fragments, then one would observe a very large anisotropy. However the experimental observations point out to a much less anisotropy. It is expected that there would be a general increase of the anisotropy in the angular distribution of the fission fragments with increasing bombarding energy and hence with the excitation energy for a particular fissioning species [10]. The simplest way to extract the relative orbital angular momentum of the fission fragments is to fit the angular distribution pattern in terms of a series of Legendre polynomials

$$\frac{W(\theta^\circ)}{W(90^\circ)} = 1 + \sum_{1=2,\text{even}} A_1 P_1(\cos\theta) - A_1 P_1(0).$$

A weighted least squares fitting is usually done taking into account the experimental uncertainties. The 1-value corresponding to the highest angular momentum component with a non-zero coefficient gives an idea of the number of units of angular momentum carried by the fission fragment.

From the angular distribution measurements, the value of K_0^2 is evaluated for each compound nucleus as a function of excitation energy in excess of the fission barrier. The general features of the variation of anisotropy with projectile bombarding energy can be worked out by the theory advanced by Bohr [8] and amplified by Strutinsky [11], Halpern and Strutinsky [12], Griffin [13] and others. According to this theory, the angular distribution $W(\theta)$ of fission fragments emitted per unit solid angle for a single fissioning species is described by the relation

$$W(\theta) \sim \int dI \int dK f(K,I) \left[\sin^2\theta - \frac{K^2}{I^2}\right]^{-1/2} \tag{1}$$

where θ is the direction of the fission fragment with respect to the beam direction, I is the angular momentum of the compound state and K is the component of angular momentum along the symmetry axis.

With the assumptions (1) that $f(K, I)$ is a product of functions $f_K(K)$ and $f_I(I)$, (2) that $f_K(K) \sim \exp(-K^2/2K_0^2)$ and (3) that $f_I(I) \sim I$ up to some limiting value I_{max} the integration of (1) results in an expression dependent upon K_0 and I_{max}. Both $W(\theta)$ and the ratio $W(\theta^\circ)/W(90^\circ)$ can be characterized by a parameter $p = (I_{\text{max}}/2K_0)^2$ [1] in

terms of which

$$\frac{W(\theta)}{W(90°)} = \frac{\int_0^p dx \dfrac{x^{1/2}\exp(-x\sin^2\theta)J_0(ix\sin^2\theta)}{\text{erf}(\sqrt{2x})}}{\int_0^p dx \dfrac{x^{1/2}\exp(-x)J_0(ix)}{\text{erf}(\sqrt{2x})}} \tag{2}$$

where J_0 is the zero-order Bessel function. Calculations based on this expression are shown in figure 3. From statistical considerations, coupled with Fermi gas model, K_0^2 is given by

$$K_0^2 = J_{\text{eff}}\, T/\hbar^2 \tag{3}$$

where T is the nuclear temperature at the saddle point and J_{eff} is the effective moment of inertia, defined as

$$J_{\text{eff}} = \frac{J_\perp J_\parallel}{(J_\perp - J_\parallel)}$$

where $J_\perp$ is the moment of inertia perpendicular to symmetry axis and $J_\parallel$ is the moment of inertia parallel to the symmetry axis. Further, T on the basis of Fermi gas model, is given by

$$T = \left[\frac{E_x^s}{a_f}\right]^{1/2} \tag{4}$$

where E_x^s and a_f are the excitation energy and nuclear level density parameter, both corresponding to the saddle point configuration of the fissioning nucleus.

Thus K_0^2 turns out to be proportional to the square root of the excitation energy E_x^s at the saddle point. I_{max}^2 taken to be equal to $2\langle I^2 \rangle_{\text{av}}$ exhibits a nearly linear dependence upon the bombarding energy of the projectile. Consequently, because the parameter $p = I_{\text{max}}^2/4K_0^2$ controls the angular anisotropy $W(\theta°)/W(90°)$, it is expected that there would be a general increase of the anisotropy in the angular distribution of the fission fragments with increasing bombarding energy, and hence with the excitation energy for a particular fissioning species.

2. Experimental details

2.1 *General*

The energetic alpha particles were obtained from the variable energy cyclotron (VEC) at Calcutta, India. The collimating system restricts the diameter of the beam at the target to $< 2\,\text{mm}$. The beam current on the target was of the order of 50 nA. The total number of alpha particles striking the target was measured by a Faraday cup (FC) equipped with a secondary electron suppression device. The connections of FC were brought out and fed to an integrator. The details of experimental procedure and detector assembly can be found in our earlier paper [4].

2.2 *Target preparation*

The thorium target was prepared by electrodeposition having thickness $= 200\,\mu\text{g/cm}^2$ of the fissionable material (ThO_2) onto a $3\,\text{mg/cm}^2$ nickel backing foil. The uranium

target was prepared by vacuum evaporation of $^{238}UO_2$ onto a $2\,mg/cm^2$ Ni-backing foil. These targets were obtained from the VEC Target Lab., Calcutta.

2.3 *Experimental observation*

The fission fragment track densities were measured for thorium and uranium targets for angles between $10°$ and $80°$ in the laboratory system. Data collected for fissioning nucleus were converted to center-of-mass coordinates assuming (1) full momentum transfer of the incident charged particle to the compound nucleus, (2) equal kinetic energy for all fission fragments and (3) symmetric fragment mass distribution. These three conditions are more or less generally satisfied in charged particle induced fission of actinide elements at medium energies as those employed in the present investigation. The kinetic energy release in the center-of-mass system was estimated from the relation [14]

$$E_K = 0.1189 \frac{Z^2}{A^{1/3}} + 7.3\,MeV$$

where E_K represents the average total kinetic energy of the fission fragments before neutron emission and Z and A are the atomic and mass numbers, respectively, of the compound nucleus.

3. Results and discussion

The analysis of the data essentially consists of the following parts:

(1) least square fitting of the center-of-mass angular distributions by a series of Legendre polynomials, to draw inferences about the relative orbital angular momentum of the fission fragments.

(2) a comparison of the asymmetry of the angular distribution for different targets as a function Z^2/A, to assess the competition between fission and neutron evaporation.

(3) determination of K_0^2 values from (5) and (6) as given below [1, 15, 4a]:

$$p = \frac{I_{max}^2}{4K_0^2} \tag{5}$$

$$\frac{W(0°)}{W(90°)} = 1 + \frac{I_{max}^2}{8K_0^2} = 1 + \frac{p}{2} \tag{6}$$

(4) measurement of the total fission cross-section by integrating the measured differential cross-sections and comparing the results with theory and previous data to resolve discrepancies and

(5) calculation of Γ_f/Γ_n from σ_f/σ_R where σ_R is the total reaction cross-section taken from the calculations of Igo and Huizenga [16, 17].

The difficulty in obtaining angular distributions to the desired accuracy is connection with a background of small tracks in the plastic track detector, which was observed in the forward hemisphere. Although the cause of such a background is not yet well understood, normally this is consistent with the expectation that in addition to fission
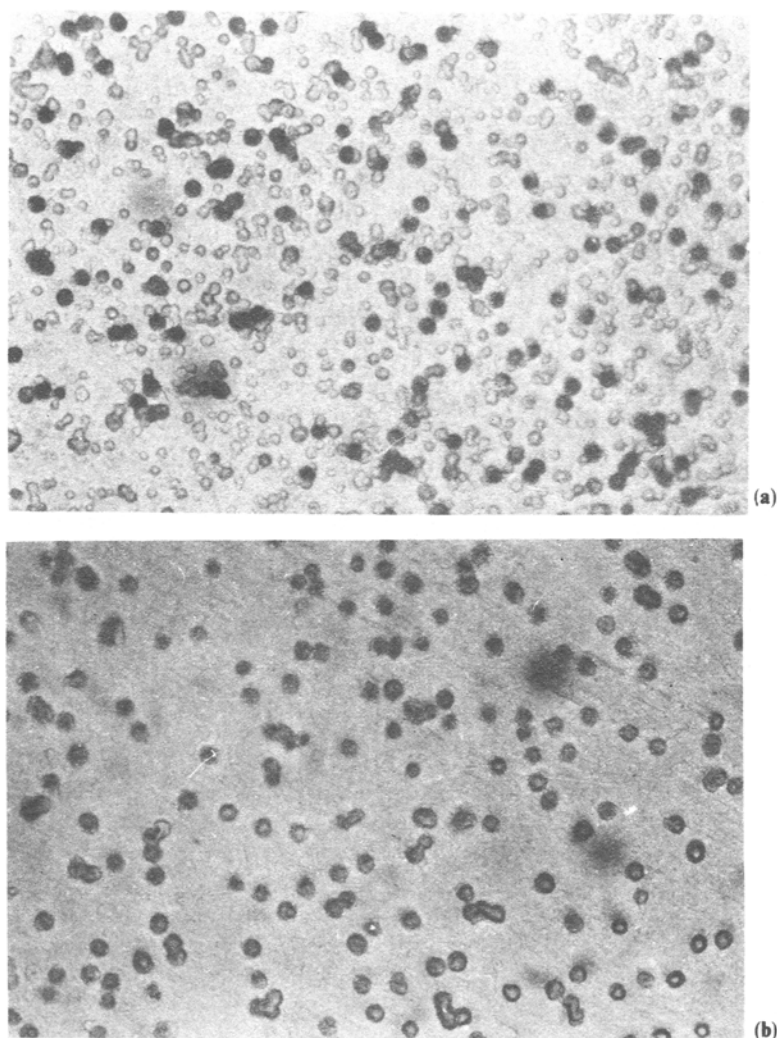
Figure 1. Photomicrographs of the fission fragment tracks in Lexan from 60 MeV He-ion induced fission of ^{232}Th (a) without covering the plastic with scotch tape, (b) after covering the plastic with scotch-tape.

fragments these would appear in the forward hemisphere due to some radioactive recoils from nuclear reactions [3]. However, these background tracks caused no difficulty in counting the fission tracks. In one particular instance where this background did become serious, the simple device of covering the plastic detector with scotch-tape dramatically reduced the background without appreciably affecting the fission tracks. Presumably the soft gum on the tape fills in the shallow "pits" on the surface. The fission tracks, being formed much deeper into the surface, were not very much affected. The microphotographs of the oriented fission tracks from the fission of thorium at 60 MeV are shown in figure 1a, b, (a) corresponds to before covering the

LEGENDRE POLYNOMIAL FIT

——●—— Th^{232}
--○-- U^{238}
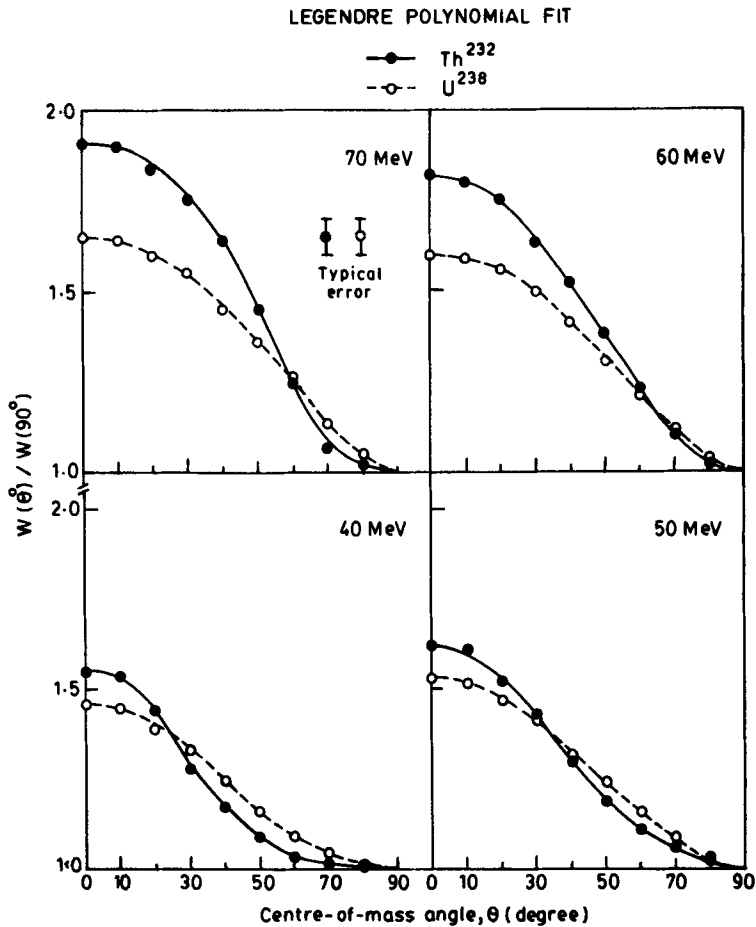
Figure 2. Angular distributions of fission fragments from the helium–ion-induced fission of ^{232}Th and ^{238}U at different incident energies of helium ion.

plastic detector with scotch-tape and (b) corresponds to after covering the plastic detector with scotch tape.

The measured track densities in the laboratory frame $W_L(\theta)$ are converted into laboratory differential cross-section $(d\sigma/d\Omega)_L$ using the formula

$$\left(\frac{d\sigma}{d\Omega}\right)_L = \frac{W_L(\theta)}{\Omega_L \phi N} \tag{7}$$

where Ω_L is the laboratory solid angle subtended by the unit area of the detector over which the track density $W_L(\theta)$ is measured, ϕ is the incident alpha particle flux and N is the number of target nuclei per unit area. The laboratory differential cross-sections are then converted into center-of-mass differential cross-sections $d\sigma/d\Omega$, using the relevant transformation equations described in our earlier paper [4]. The relative differential fission cross-section $(d\sigma(\theta°)/d\Omega)/(d\sigma(90°)/d\Omega)$ or angular anisotropies $W(\theta°)/W(90°)$ as

Table 1. Anisotropy, Z^2/A and coefficients of Legendre polynomial terms resulting from least square fit of center-of-mass angular distributions from ^{232}Th and ^{238}U.

Target	Energy (Lab) MeV	$\dfrac{W(10°)}{W(90°)}$	Z^2/A	A_0	A_2	A_4	A_6
^{232}Th	40	1·54 ± 0·06	35·86	1·1076 ± 0·0240	0·3023 ± 0·0136	0·136 ± 0·0155	0·0240 ± 0·0203
	50	1·61 ± 0·06	35·86	1·2369 ± 0·0260	0·3900 ± 0·0145	−0·0942 ± 0·0162	0·0211 ± 0·0213
	60	1·80 ± 0·07	35·86	1·2928 ± 0·0320	0·5643 ± 0·0164	−0·0315 ± 0·0183	−0·0036 ± 0·0237
	70	1·91 ± 0·07	35·86	1·3320 ± 0·0360	0·6786 ± 0·0170	−0·0369 ± 0·0187	−0·0674 ± 0·0242
^{238}U	40	1·45 ± 0·05	36·51	1·1388 ± 0·0312	0·3006 ± 0·0135	0·0268 ± 0·0154	−0·0045 ± 0·0201
	50	1·52 ± 0·05	36·51	1·1939 ± 0·0300	0·3391 ± 0·0135	−0·0281 ± 0·0158	0·044 ± 0·0201
	60	1·59 ± 0·06	36·51	1·2400 ± 0·0300	0·4168 ± 0·0144	−0·0660 ± 0·0163	0·018 ± 0·0213
	70	1·64 ± 0·06	36·51	1·2700 ± 0·0600	0·4496 ± 0·0146	−0·0967 ± 0·0165	0·0324 ± 0·0215

a function of angle θ were deduced for thorium and uranium targets and shown in figure 2 for different energies.

The solid and dashed lines in figure 2 for ^{232}Th and ^{238}U respectively are the best fit to the experimental data obtained using Legendre polynomials with terms up to $P_6(\cos\theta)$ with coefficients as tabulated in table 1. Coefficients higher than A_6 were found to be statistically not significant and hence not included in the table.

The dashed line in figure 3 indicates $(\sin\theta)^{-1}$ variation of the anisotropy as expected from a classical model in which all the angular momentum brought in by the incident particle is delivered to the fission fragments and appears as their relative orbital angular momentum. Mathematically in terms of Legendre polynomials the variation of the anisotropy is expressed as [3]

$$\frac{W(\theta°)}{W(90°)} = \frac{1}{\sin\theta} = 1 + 1·25\,P_2 + 1·27\,P_4 + 1·27\,P_6 \tag{8}$$

Comparing these coefficients with the experimentally observed coefficients listed in table 1, one can see that higher angular momentum components in the experimentally observed distributions drop off rapidly as compared to those in $(\sin\theta)^{-1}$. This is an indication that the observed relative orbital angular momentum of the fission fragments is much smaller than the actual angular momentum brought in by the incident particle.

In an approximate way, one may expect the average orbital angular momentum of the fission fragments to be given by the 1 value of the highest angular momentum term (with statistically significant coefficient) in the Legendre polynomial expansion. On this
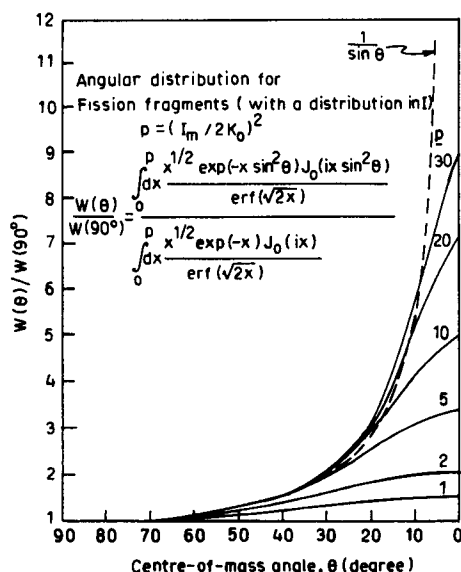
Figure 3. Calculated angular distributions for fission fragments obtained by summing over a classical sharp cut-off distribution of I (from 0 to I_{max}) (Vaz and Alexander [1]).

basis and looking at table 1, one can conclude that in the presently studied alpha induced fission of ^{232}Th and ^{238}U, the orbital momentum of the fission fragments generally does not exceed $3\hbar$ while the average incident angular momentum is about $20\hbar$. The difference between the two values is dissipated into the formation of high spin states of the fission fragments as well as into collective rotational degrees of freedom such as rolling friction in some cases.

The experimental anisotropy may be conveniently defined as $W(10°)/W(90°)$ and is listed in table 1 as a function of the parameter Z^2/A for the two fissioning nuclei at different energies. It can be seen from table 1 that the anisotropy $W(10°)/W(90°)$ increases with increase of incident particle energy; on the other hand $W(10°)/W(90°)$ decreases with increasing value of Z^2/A of the target nucleus. This trend is generally observed experimentally, but the correlation between anisotropy and Z^2/A cannot be described from the theoretical stand point as fundamental to the fission process. On the other hand, it is mostly likely to arise from fortuitous effects connected with neutron evaporation before fission.

To check the systematics of the present experiment, we deduced the value of K_0^2 which is the standard deviation of the angular momentum projection on the nuclear symmetry axis in the saddle point configuration, which sensitively controls the fission fragment angular distribution. For this purpose we used (5) and (6). The value of K_0^2 from (5) matches well with the value of K_0^2 derived from (6). For calculation the value of K_0^2 and parameter p has been taken from the figure 3 corresponding to the experimental anisotropy, which has been measured in the present experimental work. The value of p has been interpolated from figure 3 corresponding to our experimental anisotropy $W(10°)/W(90°)$. For example, in case of alpha induced fission of ^{232}Th at 40 MeV, we have taken the value of $p \simeq 1\cdot 11$ (from figure 3) corresponding to the value of experimental anisotropy $\simeq 1\cdot 54$. Values of I_{max} are estimated from the fusion cross-section code FRANPIE Vaz [18] which utilises empirical fusion barriers from Vaz *et al* [19] and (for high energies) the critical radius approach of Galin *et al* [20]. Values of I_{max}, p and K_0^2 are shown in table 2 corresponding to incident particle

Table 2. Values of I_{max} angular momentum, p-parameter corresponding to aniso-tropy $(W(10°)/W(90°))$ and K_0^2 obtained by the eqs (5) and (6) for the various energies of alpha particles.

Target	Energy (MeV)	Value of I_{max} ($\hbar$)	Value of p-parameter taken from figure 3 (corresponds to anisotropy)	Value of K_0^2 $\dfrac{W(0°)}{W(90°)} = 1 + \dfrac{I_{max}^2}{8K_0^2}$(eq (6))	$p = \dfrac{I_{max}^2}{4K_0^2}$(eq. (5))
^{232}Th	40	19	1·11	82	81
	50	23	1·26	107	105
	60	26	1·65	103	102
	70	28	1·80	106	109
^{238}U	40	19	0·92	98	98
	50	23	1·00	125	132
	60	26	1·20	141	141
	70	28	1·30	151	151

energies. From table 2, it can be noted that the value of K_0^2 increases with increasing particle energy and the value of K_0^2 in the fission of $(\alpha + {}^{238}U)$ system is greater than that of $(\alpha + {}^{232}Th)$ system.

The integral cross-section for fission at a given energy of the projectile σ_f can be determined by integration, over the solid angle, as follows [5],

$$\sigma_f = \frac{2\pi W(90°)}{\phi N\Omega} \int_0^\pi \frac{W(\theta)}{W(90°)} \sin\theta \, d\theta$$

where ϕ is the flux of bombarding particles, N is the number of target nuclei per cm^2, $W(90°)$ is the number of tracks detected at 90° in the center-of-mass coordinator system, Ω is the solid angle subtended by the detector, $W(\theta)/W(90°)$ is the center-of-mass angular distribution for the particular energy of the charged particle involved and the integration is made over 2π steradians.

The experimentally measured cross-sections are listed in table 3 for ${}^{232}Th$ and ${}^{238}U$ targets. The errors associated with the (α, f) cross-sections are estimated to be nearly 5% for thorium as well as uranium target. The measurements of some of these fission cross-sections have been made by different methods by different authors. The results of those measurements are shown in figure 4 for comparison with the present data. It can be seen that there are wide discrepancies in the fission cross-section measured by different authors with different detectors. In case of $(\alpha + {}^{232}Th)$ system, Jungerman, Hicks *et al* [21, 22] and Ford and Leachman [23] measured the fission cross-section up to only 42 MeV. Ralarosy *et al* [24] measured the fission cross-sections at different energies. If we interpolate the data of Ralarosy *et al* [24] then our present results serve to confirm the experimental results of Ralarosy *et al* [24] for ${}^{238}U(\alpha, f)$ as well as for ${}^{232}Th(\alpha, f)$. However, in the case of ${}^{238}U(\alpha, f)$, the measured fission cross-sections are found to be less than that measured by Kapoor *et al* [2]. But at 40 MeV, our result matches well with the results of Kapoor *et al* [2], Jungerman [21], Colby *et al* [25], Viola and Sikkeland [26] and Wing *et al* [27]. In both cases, ${}^{232}Th$ and ${}^{238}U$, the measured fission cross-sections are found to be very close to the total optical model reaction cross-section due to Blatt and Weisskopf [28]. This shows the predominance of the fission process in actinide elements even at high bombarding energies.

The fission cross-sections presented in figure 4 and listed in table 3 can be used to deduce quantitative information on the ratio of the partial widths for fission and neutron emission. The steep excitation functions (see figure 4) suggest that the measured fission cross-sections are mostly due to first chance fission. Therefore the fission with Γ_f is very nearly equal to the fission cross-section σ_f. Charged particle emission can be ignored at these moderate energies and therefore the neutron emission width Γ_f can be approximated with the total reaction cross-section σ_R. Thus

$$\Gamma_f/\Gamma_n \approx \sigma_f/\sigma_R. \tag{9}$$

The experimental values of Γ_f/Γ_n as a function of incident particle energy for ${}^{232}Th$ and ${}^{238}U$ are listed in table 3. The total reaction cross sections were calculated as discussed earlier. From table 3 one can notice that all the values of Γ_f/Γ_n are nearly equal to one. This also shows the predominance of the fission process in actinide elements.

Table 3. Experimental fission and calculated reaction cross-sections for alpha particle induced fission of ^{232}Th and ^{238}U.

Target	Energy (MeV)	Fission cross-section σ_f (cm^2)	Calculated reaction cross-section σ_R (cm^2)	$\Gamma_f/\Gamma_n \approx \sigma_f/\sigma_R$	Blatt and Weisskopf [28] σ_R(cm^2)
^{232}Th	40	$(1\cdot15 \pm 0\cdot06) \times 10^{-24}$	$1\cdot50 \times 10^{-24}$	$0\cdot76$	$1\cdot2 \times 10^{-24}$
	50	$(1\cdot25 \pm 0\cdot06) \times 10^{-24}$	$2\cdot00 \times 10^{-24}$	$0\cdot62$	$1\cdot6 \times 10^{-24}$
	60	$(1\cdot52 \pm 0\cdot07) \times 10^{-24}$	$2\cdot20 \times 10^{-24}$	$0\cdot69$	$1\cdot8 \times 10^{-24}$
	70	$(1\cdot65 \pm 0\cdot08) \times 10^{-24}$	$2\cdot35 \times 10^{-24}$	$0\cdot70$	$2\cdot0 \times 10^{-24}$
^{238}U	40	$(1\cdot46 \pm 0\cdot07) \times 10^{-24}$	$1\cdot70 \times 10^{-24}$	$0\cdot86$	$1\cdot5 \times 10^{-24}$
	50	$(1\cdot65 \pm 0\cdot08) \times 10^{-24}$	$2\cdot15 \times 10^{-24}$	$0\cdot76$	$1\cdot8 \times 10^{-24}$
	60	$(1\cdot98 \pm 0\cdot10) \times 10^{-24}$	$2\cdot33 \times 10^{-24}$	$0\cdot85$	$2\cdot0 \times 10^{-24}$
	70	$(2\cdot10 \pm 0\cdot10) \times 10^{-24}$	$2\cdot62 \times 10^{-24}$	$0\cdot80$	$2\cdot3 \times 10^{-24}$
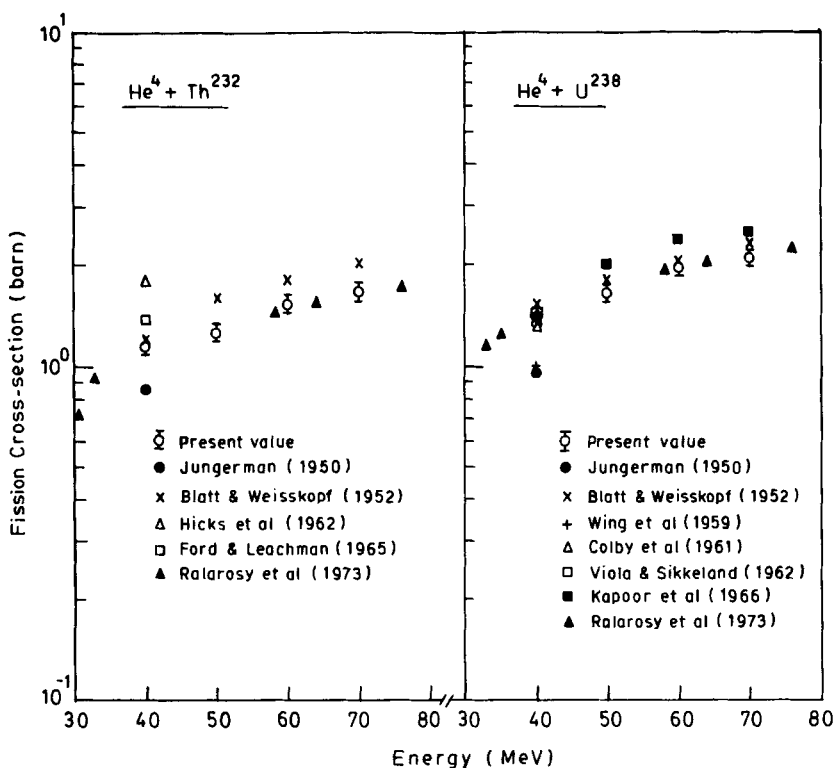
Figure 4. Measured fission cross-section at different alpha bombarding energies for the case of alpha induced fission of ^{232}Th and ^{238}U and other author's values for the same energies.

References

[1] L C Vaz and J M Alexander, *Phys. Rep.* **97**, 1 (1983)
[2] S S Kapoor, H Baba and S G Thompson, *Phys. Rev.* **149**, 965 (1966)
[3] C T Coffin and I Halpern, *Phys. Rev.* **112**, 536 (1958)
[4] R K Jain, J Rama Rao and S K Bose, *Pramana – J. Phys.* **39**, 85 (1992)
[4a] R K Jain, Ch V Sastry, J Rama Rao and S K Bose, *DAE Symp. on Nucl. Phys.* **B35**, 290 (1992)
[5] R K Jain, J Rama Rao and S K Bose, *Indian J. Phys.* **A67**, 149 (1993)
[6] R Vandenbosch, H Warharek and J R Huizengs, *Phys. Rev.* **124**, 846 (1961)
[7] R H Iyer, A K Pandey, P C Kalsi and R C Sharma, *Phys. Rev.* **C44**, 2644 (1991)
[8] A Bohr, *Proc. Int. Conf. Peaceful uses of atomic energy*, Geneva Paper P/911, (1955)
[9] R Vandenbosch and J R Huizenga, *Nuclear Fission* (New York, Academic, 1973)
[10] S S Kapoor and V S Ramamurthy, *Pramana – J. Phys.* **33**, 161 (1989)

[11] V M Strutinski, *Eksptl. i Teoret. Fiz.* **30**, 606 (1957); *Atomnaya Energi* **2**, 508; *Sov. J. Atomic Energy* **2**, 621 (1957)

[12] I Halpern and V M Strutinsky, *Proc. Int. Conf. Peaceful uses of Atomic Energy*, Geneva (1958) **15**, p. 408

[13] J J Griffin, *Phys. Rev.* **116**, 107 (1959)

[14] V E Viola, K Kwiatkowski and M Walker, *Phys. Rev.* **C31**, 1550 (1985)

[15] R H Iyer, A K Pandey, P C Kalsi and R C Sharma, *DAE Symp. on Nucl. Phys.* **B33**, 111 (1990)

[16] G Igo, *Phys. Rev.* **115**, 1665 (1959)

[17] J R Huizenga and G Igo, *Nucl. Phys.* **29**, 462 (1962)

[18] L C Vaz, *Computer Phys. Commun.* **22**, 451 (1981)

[19] L C Vaz, J M Alexander and G R Satchler, *Phys. Rep.* **69**, 373 (1981)

[20] J Galin, D Guerreau, M Lefort and X Tarrago, *Phys. Rev.* **C9**, 1018 (1974)

[21] J Jungerman, *Phys. Rev.* **79**, 632 (1950)

[22] H G Hicks, H B Levy, W E Nervik, P C Stevenson, J B Niday and J C Amstrong, *Phys. Rev.* **128**, 700 (1962)

[23] G P Ford and R B Leachman, *Phys. Rev.* **B137**, 826 (1965)

[24] J Ralarosy, M Debeauvais, G Remy, J Tripier, R Stein and D Huss, *Phys. Rev.* **C8**, 2372 (1973)

[25] L J Colby, M Lasalle Shoaf and J N Cobble, *Phys. Rev.* **121**, 1415 (1961)

[26] V E Viola and T Sikkeland, *Phys. Rev.* **128**, 767 (1962)

[27] J Wing, W J Ramler, A L Harkness, J R Huizenga, *Phys. Rev.* **114**, 163 (1959)

[28] J M Blatt and V F Weisskopf, *Theoretical nuclear physics* (New York, Wiley, 1952)